# Stereo and Calibration

# Camera Calibration of a Head-Eye System for Active Vision

Mengxiang Li

Computational Vision and Active Perception Laboratory (CVAP)
Department of Numerical Analysis and Computing Science
Royal Institute of Technology (KTH), S-100 44 Stockholm, Sweden
Email: mxli@bion.kth.se

**Abstract.** In this paper, we present methods and techniques for calibrating cameras of a head-eye system, which has computer controlled focusing, zooming, and iris. The idea is to build up look-up-tables for intrinsic parameters so we can index them. Extensive experiments were carried out and results are reported here.

## 1 Introduction and Background

Camera calibration is useful, if not necessary, in many vision problems, e.g., 3D reconstruction from stereo, vergency, fixation, etc. This problem usually involves two parts. The first part is to determine internal parameters of a camera, the so-called *intrinsic* parameters, such as focal length, lens distortion, principal point, and aspect ratio of the pixel array. The second part is the pose estimation of a camera (system) relative to a 3–D world reference system, including rotation and translation between these two systems. These are the so-called *extrinsic* parameters.

In an *active vision* system, i.e., a visual system which is able to manipulate its visual parameters in a controlled manner [9], one changes (manipulates) the visual parameters of the system all the time. At any time one wants to know the intrinsic as well as the extrinsic parameters of the system in order to perform certain vision tasks. This imposes difficulties for camera calibration. It is difficult to perform real-time calibration, if possible at all. On the other hand, the movements of the system are controlled, i.e., we know how much we moved relatively from some initial position. If we pre-calibrate the system, we can then compute (index) the parameters at any time. In this way, we can perform "real-time" calibration. Fig. 1(a) shows the KTH head-eye system, which consists of a pair of cameras (eyes) mounted on a head and the head is mounted on a shoulder (platform). The system has 13 degrees of freedom, see [8] and [9] for details. In this paper, we address the first part of the calibration of the system, i.e., the calibration of intrinsic parameters and try to build up look-up-tables for them. The second part of the calibration, i.e., the dynamic pose estimation or the kinematic calibration, is addressed in [7].

In our study, we use a *pin-hole* camera model, as depicted in Fig. 1(b). The pin-hole model does not hold for zoom lens [10, 5], but for a fixed zoom, the lens

Lecture Notes in Computer Science, Vol. 800
Jan-Olof Eklundh (Ed.)
Computer Vision – ECCV '94

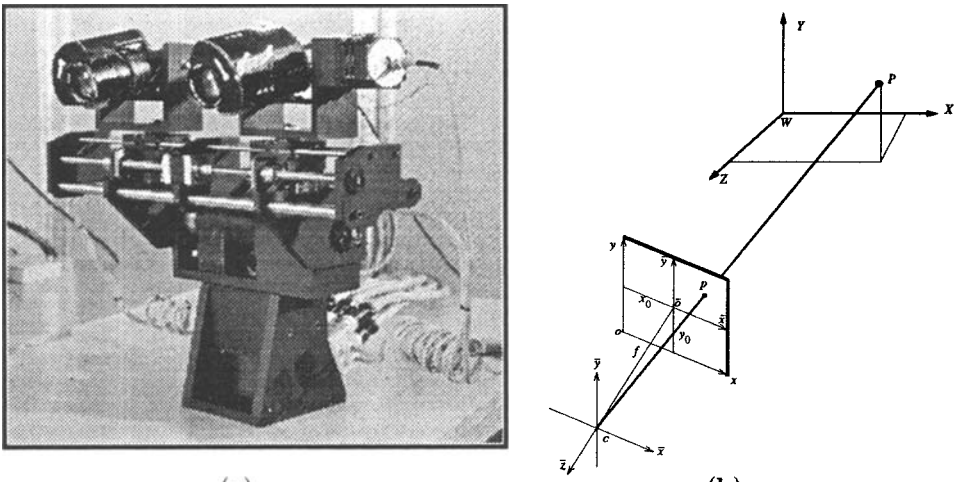


(a) (b)

**Fig. 1.** (a) *The KTH-head-eye system.* (b) *The pin-hole camera model, image geometry and coordinate systems.*

system can be abstracted as a pin-hole model. Through this paper, the following notations are used. $W$–$XYZ$ is a 3D world reference system. $o$–$xy$ is a 2D image pixel system with origin at the low-left corner of the image. $\bar{o}$–$\bar{x}\bar{y}$ is a 2D image coordinate system with $\bar{x}$ and $\bar{y}$ parallel to the ones of $o$–$xy$ and with origin at the principal point $\bar{o}$. $c$–$\bar{x}\bar{y}\bar{z}$ is a 3D camera coordinate with origin at the optical center $c$, $\bar{z}$-axis coincides with the optical axis and $\bar{x}$, $\bar{y}$ parallel to the ones of $\bar{o}$–$\bar{x}\bar{y}$.

## 2 Principal Point Calibration by Focusing/Zooming

Principal point is defined as the intersection point of optical axis and image plane. Under the pin-hole camera model, focusing and zooming is equivalently to change distance between optical center and image plane, see Fig. 2. When focusing or zooming, each image point will move radiately along a line passing through the principal point. If we take a sequence of images by changing focus and/or zooming, find the corresponding image points on each image and overlay them together, Fig. 2.(b), the lines determined by the same image point at different images will intersect at a common point, which is the principal point. In practice, due to various errors, the lines will not intersect precisely at a common point, a least squares estimation may be used to determine the common intersection point, i.e., the principal point. This technique has been proposed by Tsai [11] and used by Lavest et. al. [5].

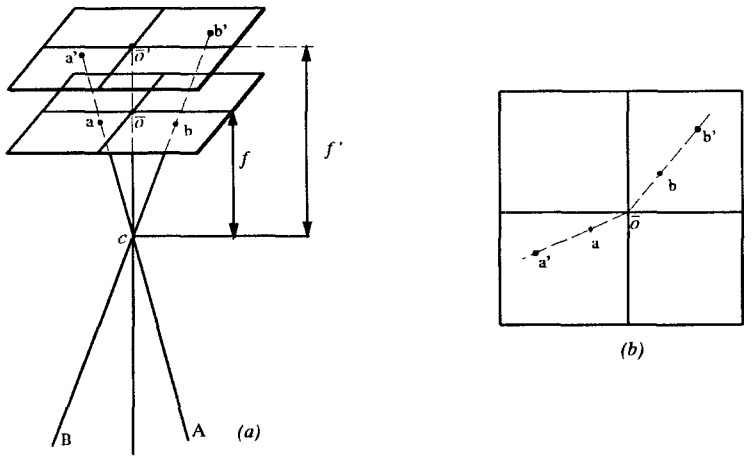


**Fig. 2.** *Determine principal point by focusing/zooming.*

## 3 Calibration Using Vanishing Points

Using vanishing point technique for camera calibration has been studied by, e.g., [2], [3], [12], and [4]. For a set of parallel line segments in 3D when projected onto an image plane, their projections (line segments) will intersect at a common point on the image plane, that is the so-called *vanishing point*. One useful property of vanishing point is that *the direction from the projection center to the vanishing point is parallel to the direction of the 3D line segments*. The basic idea is to using three vanishing points of three orthogonal groups of parallel lines in 3D space to recover some of the intrinsic parameters and the rotation matrix. The advantage of this technique is that it is relatively simple to reconstruct such a calibration object and parameters can be computed in closed form. One drawback is that it does not allow a full intrinsic and extrinsic parameters calibration (the translation vector cannot be computed from vanishing points) and the accuracy is limited.

### 3.1 Calibrating Intrinsic Parameters

Given three sets of multi-orthogonal parallel lines in 3D space: $\boldsymbol{G}_1$, $\boldsymbol{G}_2$, and $\boldsymbol{G}_3$, see Fig. 3, and their corresponding vanishing points on the image plane: $g_1(x_1, y_1)$, $g_2(x_2, y_2)$, and $g_3(x_3, y_3)$. Let the principal point be $(x_0, y_0)$, the focal length be $f$, and the scale factors of pixel array be $s_x, s_y$. Then the three vanishing point vectors (not unit) in the camera system are:

$$\left.\begin{aligned} \boldsymbol{g}_1 &= [(x_1 - x_0)s_x, (y_1 - y_0)s_y, -f]^T \\ \boldsymbol{g}_2 &= [(x_2 - x_0)s_x, (y_2 - y_0)s_y, -f]^T \\ \boldsymbol{g}_3 &= [(x_3 - x_0)s_x, (y_3 - y_0)s_y, -f]^T \end{aligned}\right\} \quad (1)$$

As $\boldsymbol{G}_1, \boldsymbol{G}_2$ and $\boldsymbol{G}_3$ are orthogonal to each other, so are $\boldsymbol{g}_1, \boldsymbol{g}_2$ and $\boldsymbol{g}_3$ according to the vanishing point property, i.e., $\boldsymbol{g}_1 \cdot \boldsymbol{g}_2 = 0$, $\boldsymbol{g}_2 \cdot \boldsymbol{g}_3 = 0$, $\boldsymbol{g}_3 \cdot \boldsymbol{g}_1 = 0$, or

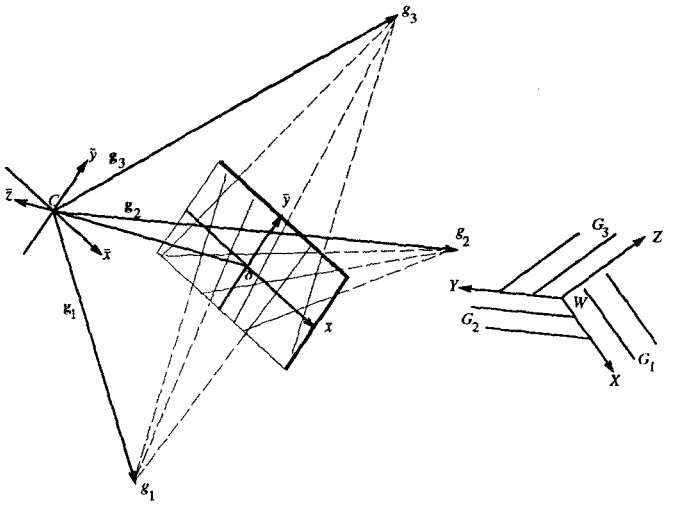


**Fig. 3.** *Geometry of vanishing points*

$$\left.\begin{aligned}(x_1-x_0)(x_2-x_0)+(y_1-x_0)(y_2-x_0)k^2+f_x^2=0\\(x_2-x_0)(x_3-x_0)+(y_2-x_0)(y_3-x_0)k^2+f_x^2=0\\(x_3-x_0)(x_1-x_0)+(y_3-x_0)(y_1-x_0)k^2+f_x^2=0\end{aligned}\right\} \tag{2}$$

where, $k=\frac{s_y}{s_x}$ is the aspect ratio of the pixel, and $f_x=\frac{f}{s_x}$ is the focal length expressed in pixel in $x$-direction. We have four parameters: $k, f_x, x_0, y_0$, but only three equations. Either we know $k$ and solve for $x_0, y_0$ and $f_x$ or we know $x_0, y_0$ and solve for $k$ and $f_x$. In both cases they can be computed directly from (2).

### 3.2 Calibrating Rotation Matrix

If we let the three multi-orthogonal vectors coincide with $X, Y$, and $Z$ axes of an object space coordinate system, we can compute the rotation matrix $\boldsymbol{R}$ directly in closed form. Let $\boldsymbol{G}_1$, $\boldsymbol{G}_2$ and $\boldsymbol{G}_3$ be in $X$, $Y$ and $Z$ direction respectively, see Fig. 3. The three unit vectors $\boldsymbol{N}_{G_1}$, $\boldsymbol{N}_{G_2}$, and $\boldsymbol{N}_{G_3}$ along $\boldsymbol{G}_1$, $\boldsymbol{G}_2$, and $\boldsymbol{G}_3$ in $W$–$XYZ$ system are: $\boldsymbol{N}_{G_1}=\boldsymbol{E}_x=(1,0,0)^T, \boldsymbol{N}_{G_2}=\boldsymbol{E}_y=(0,1,0)^T, \boldsymbol{N}_{G_3}=\boldsymbol{E}_z=(0,0,1)^T$. On the other hand, we have their corresponding unit vanishing point vectors in the camera system: $\boldsymbol{n}_{g_1}=\frac{\boldsymbol{g}_1}{|\boldsymbol{g}_1|}, \boldsymbol{n}_{g_2}=\frac{\boldsymbol{g}_2}{|\boldsymbol{g}_2|}, \boldsymbol{n}_{g_3}=\frac{\boldsymbol{g}_3}{|\boldsymbol{g}_3|}$. As $\boldsymbol{n}_{g_i}$ is the rotated result of $\boldsymbol{N}_{G_i}$ by rotation matrix $\boldsymbol{R}$, so we have:

$$\left.\begin{aligned}\boldsymbol{n}_{g_1}&=\boldsymbol{R}\,\boldsymbol{N}_{G_1}=\boldsymbol{R}\,\boldsymbol{E}_x\\\boldsymbol{n}_{g_2}&=\boldsymbol{R}\,\boldsymbol{N}_{G_2}=\boldsymbol{R}\,\boldsymbol{E}_y\\\boldsymbol{n}_{g_3}&=\boldsymbol{R}\,\boldsymbol{N}_{G_3}=\boldsymbol{R}\,\boldsymbol{E}_z\end{aligned}\right\} \tag{3}$$

Then the rotation matrix $\boldsymbol{R}$ can be computed directly from (3):

$$\boldsymbol{R}=(\boldsymbol{n}_{g_1},\boldsymbol{n}_{g_2},\boldsymbol{n}_{g_3}) \tag{4}$$

# 4 Simultaneously Calibration by Least Squares Technique

## 4.1 The Mathematical Model

The transformation from object space to image space can be expressed as:

$$\bar{\boldsymbol{x}}_i = \lambda_i \boldsymbol{R}(\boldsymbol{X}_i - \boldsymbol{T}) \tag{5}$$

where in (5), $\bar{\boldsymbol{x}}_i = (\bar{x}_i, \bar{y}_i, \bar{z}_i)^T$ is an image point in the camera system as defined in Fig. 1 and $-\bar{z}_i \equiv f$, i.e., the focal length of the camera, $\lambda_i$ is a scale factor which maps a point in object space to the image plane, $\boldsymbol{X}_i = (X_i, Y_i, Z_i)^T$ is an point in $W$–$XYZ$ system, $\boldsymbol{T} = (T_x, T_y, T_z)^T$ is the translation vector, and $\boldsymbol{R}$ is the rotation matrix, which is represented here by three rotation angles: $\alpha$ around $X$-axis, $\beta$ around $Y$-axis, and $\gamma$ around $Z$-axis. Eliminating $\lambda_i$ in (5) and omit the subscript $i$, we have:

$$\left.\begin{aligned} \bar{x} &= -f\frac{r_{11}(X-T_x)+r_{12}(Y-T_y)+r_{13}(Z-T_z)}{r_{31}(X-T_x)+r_{32}(Y-T_y)+r_{33}(Z-T_z)} \\ \bar{y} &= -f\frac{r_{21}(X-T_x)+r_{22}(Y-T_y)+r_{23}(Z-T_z)}{r_{31}(X-T_x)+r_{32}(Y-T_y)+r_{33}(Z-T_z)} \end{aligned}\right\} \tag{6}$$

Transforming $(\bar{x}, \bar{y})$ into the pixel coordinate system $(x, y)$, that is

$$\left.\begin{aligned} \bar{x} &= (x + v_x - x_0 - dx_r - dx_t)s_x \\ \bar{y} &= (y + v_y - y_0 - dy_r - dy_t)s_y \end{aligned}\right\} \tag{7}$$

here $v_x, v_y$ are measurement errors of $x$, $y$. $(dx_r, dy_r)$ are *radial* distortion components and $(dx_t, dy_t)$ are *tangential* distortion components. We use two models which are often used in photogrammetry [1]:

$$\left.\begin{aligned} dx_r &= (x - x_0)(a_1 r^2 + a_2 r^4 + a_3 r^6) \\ dy_r &= (y - y_0)(a_1 r^2 + a_2 r^4 + a_3 r^6) \end{aligned}\right\} \tag{8}$$

$$\left.\begin{aligned} dx_t &= \Big[p_1[r^2 + 2(x - x_0)^2] + 2p_2(x - x_0)(y - y_0)\Big](1 + p_3 r^2) \\ dy_t &= \Big[p_2[r^2 + 2(y - y_0)^2] + 2p_1(x - x_0)(y - y_0)\Big](1 + p_3 r^2) \end{aligned}\right\} \tag{9}$$

where in (7), (8), and (9), $x_0, y_0$ are the principal point in the pixel system, $a_1, a_2, a_3$ are the radial lens distortion parameters, $p_1, p_2, p_3$ are the tangential distortion parameters, and $s_x, s_y$ are the scale factors of pixel system in $x$ and $y$ directions respectively, and $r$ is the radial distance from the principal point. Let $f_x = \frac{f}{s_x}$, $f_y = \frac{f}{s_y}$, substituting (7), (8) and (9) into (6), it becomes:

$$\left.\begin{aligned} x + v_x &= x_0 + dx_r + dx_t - f_x\frac{r_{11}(X-T_x)+r_{12}(Y-T_y)+r_{13}(Z-T_z)}{r_{31}(X-T_x)+r_{32}(Y-T_y)+r_{33}(Z-T_z)} = \mathcal{F}_x(\boldsymbol{\Phi}) \\ y + v_y &= y_0 + dy_r + dy_t - f_y\frac{r_{21}(X-T_x)+r_{22}(Y-T_y)+r_{23}(Z-T_z)}{r_{31}(X-T_x)+r_{32}(Y-T_y)+r_{33}(Z-T_z)} = \mathcal{F}_y(\boldsymbol{\Phi}) \end{aligned}\right\} \tag{10}$$

here $\boldsymbol{\Phi}$ is the parameter vector, i.e.,$\boldsymbol{\Phi} = [(x_0, y_0, a_1, a_2, a_3, p_1, p_2, p_3, f_x, f_y); (T_x, T_y, T_z, \alpha, \beta, \gamma)]^T$. The first part is the intrinsic parameters and the second part is the extrinsic parameters. The problem is now to solve for $\boldsymbol{\Phi}$ through

$$\min_{\boldsymbol{\Phi} \in \Re^{16}} \sum_{i=1}^{n} (v_{x_i}^2 + v_{y_i}^2) \tag{11}$$

In (10) $\mathcal{F}_x(\boldsymbol{\Phi})$ and $\mathcal{F}_y(\boldsymbol{\Phi})$ are non-linear functions of $\boldsymbol{\Phi}$, the minimization is a non-linear problem. One way of solving it is to linearize (10) with some initial value $\boldsymbol{\Phi}_0$ and solve for $\boldsymbol{\Delta\Phi}$. Then by adding $\boldsymbol{\Delta\Phi}$ to $\boldsymbol{\Phi}_0$ as new approximate values we solve for new $\boldsymbol{\Delta\Phi}$. Repeating this until convergency is reached.

### 4.2 Multi-image Calibration

One major source of errors in calibration is the measurement errors. In order to increase accuracy, one can use more than one image taken by the same camera from the same or different positions. In such a case, the intrinsic parameters are the same for all images and some of the extrinsic parameters are the same as well (if the camera is not moved). By simulations, it is found that accuracy increases linearly with the increasing of number of images, see [6] for details. The multi-image technique has also been suggested by Tsai [11].

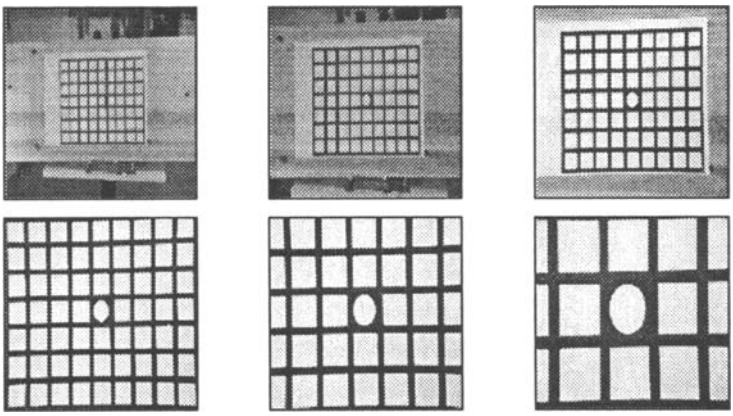

**Fig. 4.** *Some examples of images used for determining principal point by zooming.*

## 5 Experiments and Results

### 5.1 Determining Principal Point by Zooming

The principal point is calibrated first separately using the zooming technique described in Section 2. A chess board pattern is used for the calibration. The zooming motor steps has been mapped to [0, 1.0] with "continuous" stepping. By keeping the calibration object still and taking image by stepping 0.05 steps, we get a sequence of 22 images of the same object, see Fig. 4 for a few examples. By extracting and tracing the same point (the corners of the rectangles) through the sequence, a number of line segments are obtained, Fig. 5 (a). By fitting line model to line segments, line parameters are computed for all the line segments. And finally, a common intersection point of all lines are computed by least squares method, Fig. 5 (b). In order to check the stability of the principal point under zooming, we chose different combinations of images to determine the intersection

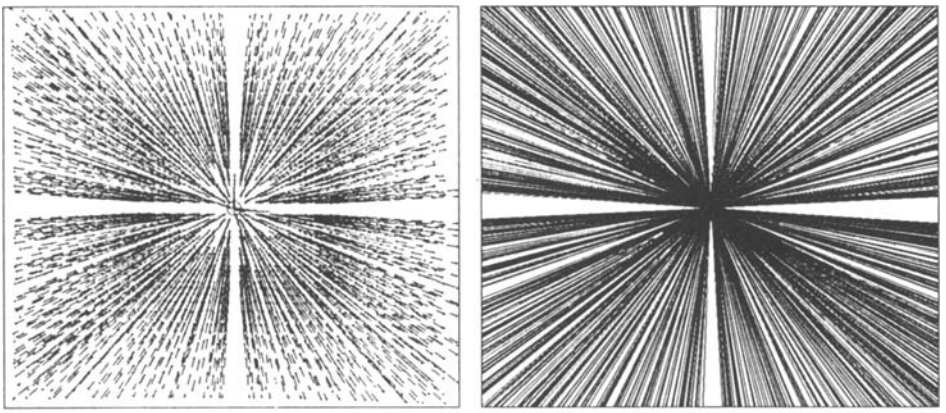


**Fig. 5.** *Determining principal point by zooming.* (a) *Line segments obtained by tracing corresponding points through the sequence of images;* (b) *intersection of line segments.*

point. Fig. 6 show the trace of principal point under zooming. As can be seen from the figure, the principal point of left camera moves almost along a line, while the right is more randomly. The figure also show the stability over different object distances, which is equivalent to different focus setups, and time as those images were taken at a time interval of 3 months.

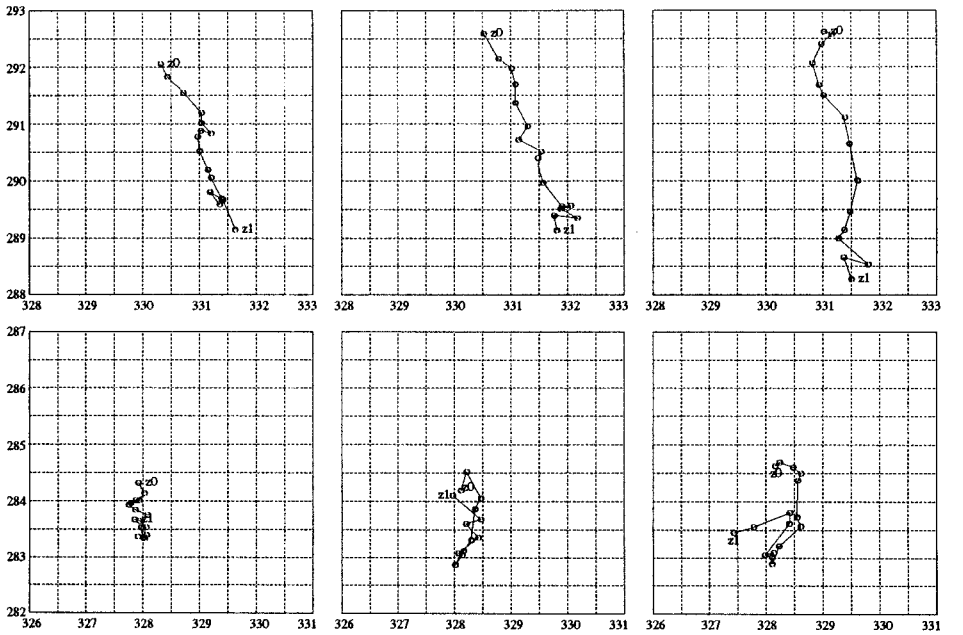


**Fig. 6.** *Shifting of principal point under zooming. Top: left camera, bottom: right camera. From left to right three experiments done at different focus setups and date.*

## 5.2 Vanishing Points and Least Squares Calibration

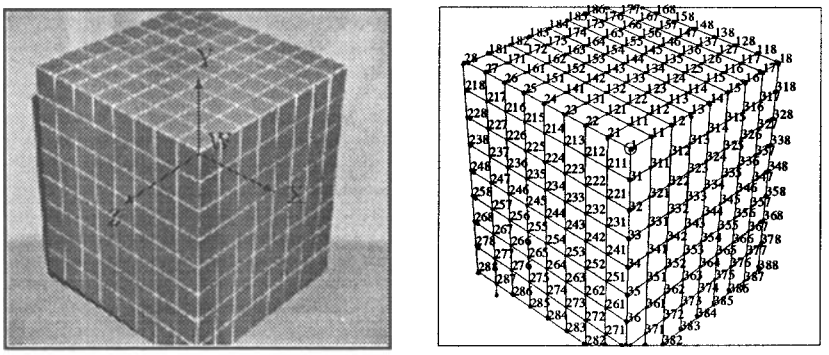

(a) (b)

**Fig. 7.** (a) *The calibration cube* $(0.4 \times 0.4 \times 0.4m^3)$ *with multi-orthogonal straight lines on each face. The three edges define a right-hand 3D co-ordinate system as a world reference system. The intersection points on each face are measured and used as 3D control points for the calibration.* (b) *The identified line segments and points.*

A cube calibration object has been constructed for the calibration (Fig. 7). First we compute camera parameters by vanishing points technique as presented in Section 3. Then using these as initial values, we perform a least squares calibration. All the calibration is made fully automatically. In the following we present results of various experiments using multiple images. All results shown here are using fixed principal points calibrated by zooming.

The first experiment is to calibrate intrinsic parameters under different zoom steps. It is done as follows: keeping the focus and iris fixed, changing zoom step by 0.1 steps [1] and take a few (five) images. These images have the same intrinsic parameters and extrinsic parameters (if the camera is not moved). Fig. 8 shows the results of the calibrated radial distortion with different zooming steps. Notice that at lower zoom step ($< 0.4$), the object on the image only covers a small part at the center, we cannot determine the distortion outside this region, rather than extrapolate them. As can be seen from the figure, the both camera's distortion varies under zooming, but for certain applications, they can be ignored within the center part of image, say $400 \times 400$ pixels, as they are less than a half pixel. (Tangential distortion can be ignored as they are very small from experiments. Due to space, they are not reported here, for detail see [6]).

Fig. 9 shows the calibrated focal lengths $f_x$ and $f_y$ under different zoom steps, both increasing exponentially. From Fig. 9 we can build up a look-up-function and index focal length at any zoom step. Fig. 10 shows the distance between the optical center and the calibration cube origin under zooming and Fig. 11 shows the trace of optical centers in space under zooming. We can see that both optical

[1] The zoom step is from 0 to 1.0, but when up to 0.8, only a small part of the cube is visible on the image. So all the experiments are done from 0 to 0.8.

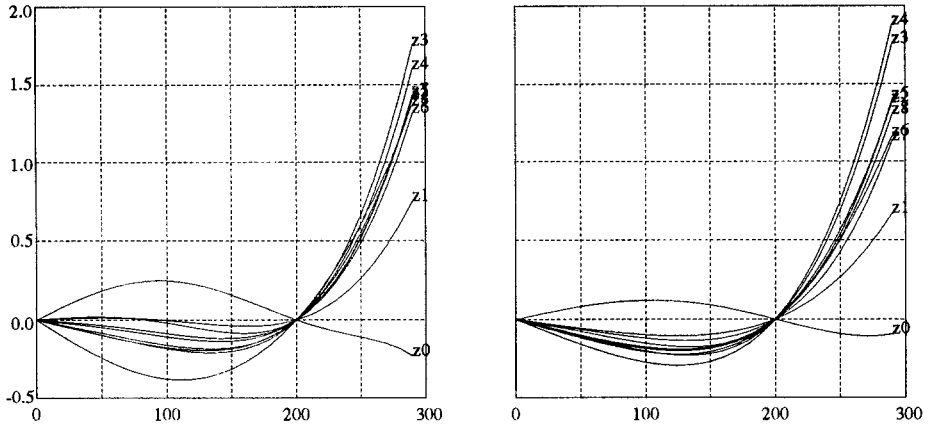


**Fig. 8.** *Recovered radial distortions for left (left) and right (right) camera.*

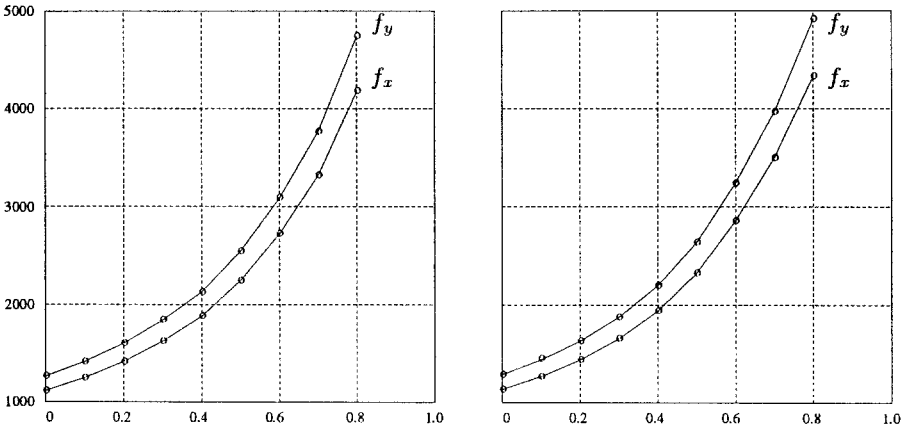


**Fig. 9.** *Calibrated focal lengths under zooming for left (left) and right (right) camera. The horizontal axes are zoom motor steps and the vertical axes are focal lengths.*

centers move along a straight line. Note that the shifting range of the optical center does not correspond to the range of the focal length. This is due to the factor that the pin-hole model does not hold for lens system, see also Lavest et. al [5]. But for a fixed zoom (each step), we can model the lens using the pin-hold model. Tab. 1 shows the results of the computed rotation angles $\alpha, \beta$, and $\gamma$ as well as the aspect ratio of the pixel array for different zoom. They are all in the expected range.

The second experiment is to see how focusing changes focal length. In normal case, changing focus means changing the image scale, thus the focal length. With a zoom lens, this change can be compensated by zoom, so the image scale is not changed when focusing. The KTH head-eye system is designed in such a way.

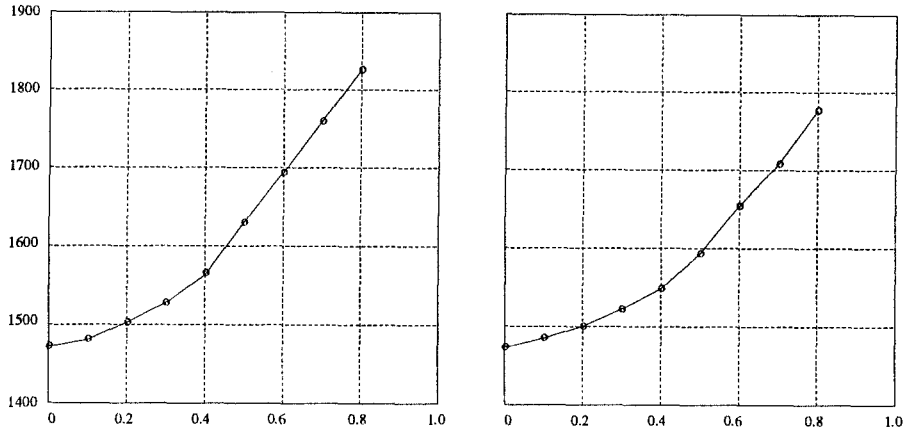


**Fig. 10.** *Distance between optical center and calibration cube (origin) under zooming.*

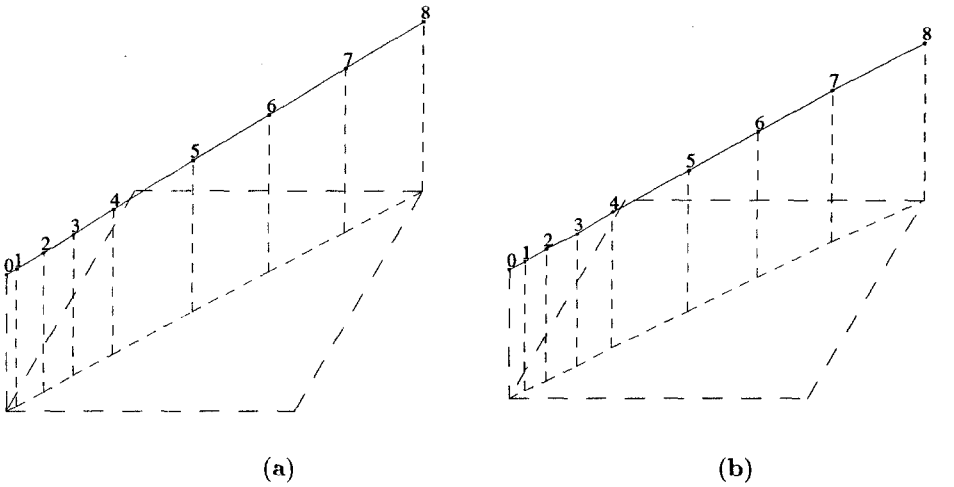


**Fig. 11.** *Trace of optical center in 3D under zooming:* **(a)** *left camera, moving range* $(861.1, 709.7, 959.9) \rightarrow (1065.4, 889.1, 1186.3)$, $D_l = 354.1mm$, *and* **(b)** *right camera, moving range* $(982.3, 711.2, 836.2) \rightarrow (1176.8, 860.7, 1015.5)$, $D_r = 310.1mm$.

But this needs to be calibrated. The result in Tab. 2 shows that the focal length changes slightly as focus changes. This results will be used the compensation.

The third experiment is to show how iris changes focal length. Tab. 3 shows the experimental results of the calibrated focal length under different iris openness. The table shows that iris does not change the focal length significantly, Iris opening changes the brightness of the image. It tends to amplify images of bright objects with dark background when increasing (open) iris and vice verse. But the amplification is a local scaling referred to the center point of the image of an object, so it does not shift nor scale the image globally.

**Table 1.** *Results of calibrated rotation angles under different zooming*

| *zoom* | *left camera* | | | | *right camera* | | | |
|---|---|---|---|---|---|---|---|---|
| *step* | $\alpha$ | $\beta$ | $\gamma$ | $k$ | $\alpha$ | $\beta$ | $\gamma$ | $k$ |
| 0.0 | -37.976 | 35.069 | 25.481 | 0.88066 | -41.122 | 40.302 | 27.248 | 0.88133 |
| 0.1 | -37.928 | 35.085 | 25.477 | 0.88109 | -41.123 | 40.295 | 27.246 | 0.88173 |
| 0.2 | -37.974 | 35.124 | 25.507 | 0.88197 | -41.102 | 40.324 | 27.236 | 0.88203 |
| 0.3 | -38.009 | 35.111 | 25.524 | 0.88234 | -41.082 | 40.344 | 27.248 | 0.88247 |
| 0.4 | -37.956 | 35.051 | 25.487 | 0.88222 | -41.161 | 40.275 | 27.290 | 0.88311 |
| 0.5 | -37.939 | 35.096 | 25.461 | 0.88212 | -41.022 | 40.202 | 27.179 | 0.88250 |
| 0.6 | -37.919 | 35.168 | 25.455 | 0.88175 | -41.089 | 40.283 | 27.200 | 0.88226 |
| 0.7 | -37.939 | 35.116 | 25.486 | 0.88213 | -40.983 | 40.231 | 27.135 | 0.88117 |
| 0.8 | -37.952 | 35.144 | 25.458 | 0.88226 | -41.165 | 40.232 | 27.286 | 0.88177 |

**Table 2.** *Results of local length calibration under different focus steps*

| *left camera* | | | *right camera* | | |
|---|---|---|---|---|---|
| *focus* | $f_x$ | $f_y$ | *focus* | $f_x$ | $f_y$ |
| 0.30 | 1752.550 | 1986.723 | 0.30 | 1653.458 | 1875.359 |
| 0.38 | 1736.127 | 1968.290 | 0.40 | 1641.583 | 1861.609 |
| 0.40 | 1740.218 | 1973.757 | 0.42 | 1635.674 | 1853.734 |
| 0.40 | 1724.895 | 1955.388 | 0.45 | 1626.711 | 1843.179 |
| 0.50 | 1698.170 | 1925.506 | 0.55 | 1620.808 | 1837.419 |
| 0.50 | 1699.129 | 1926.061 | 0.55 | 1622.913 | 1840.618 |
| 0.50 | 1703.694 | 1931.364 | 0.60 | 1607.567 | 1823.694 |

## 6 Discussion and Conclusions

We have presented different methods and techniques for camera calibration and some experimental results for calibrating the KTH-head system. We also developed procedures for automatically calibrating the system. The results show that the intrinsic parameters of the head-eye system can be pre-calibrated and built into look-up-tables. The accuracy and stability of the calibration depends on the calibration techniques and the system itself. For certain applications in which accuracy is not a crucial point, the intrinsic parameters can be indexed from LUTs without on-the-job calibration. This is important for real-time system, e.g., an active vision system.

### Acknowledgements

The work presented here was performed under the ESPRIT-BRA 7108 *Vision as Process* (VAP-II) project. The support from the Swedish National Board for Industrial and Technical Development, NUTEK, is gratefully acknowledged.

**Table 3.** *Results of calibrated local length under different iris*

| iris | *left camera* | | | | *right camera* | | | |
|---|---|---|---|---|---|---|---|---|
| | $f_x$ | $\sigma_{f_x}$ | $f_y$ | $\sigma_{f_y}$ | $f_x$ | $\sigma_{f_x}$ | $f_y$ | $\sigma_{f_y}$ |
| *close* | 2076.624 | 6.307 | 2353.643 | 7.272 | 2008.574 | 6.039 | 2278.094 | 6.977 |
| | 2078.534 | 6.554 | 2355.619 | 7.543 | 2009.312 | 6.124 | 2279.302 | 7.074 |
| | 2077.240 | 6.835 | 2354.535 | 7.874 | 2005.799 | 6.187 | 2274.635 | 7.161 |
| | 2076.165 | 6.615 | 2352.980 | 7.628 | 2005.865 | 6.218 | 2274.602 | 7.196 |
| ↓ | 2079.249 | 6.928 | 2356.932 | 7.983 | 2007.321 | 6.379 | 2276.079 | 7.382 |
| | 2075.862 | 7.142 | 2353.552 | 8.230 | 2007.529 | 6.397 | 2276.386 | 7.385 |
| | 2082.139 | 7.009 | 2359.002 | 8.090 | 2009.249 | 6.677 | 2279.019 | 7.702 |
| | 2080.316 | 7.591 | 2356.396 | 8.765 | 2008.732 | 7.739 | 2277.815 | 8.925 |
| | 2078.521 | 8.228 | 2354.087 | 9.500 | 2007.367 | 7.751 | 2277.165 | 8.962 |
| *open* | 2078.557 | 9.137 | 2355.187 | 10.491 | 2009.648 | 8.003 | 2278.350 | 9.276 |

# References


1. ASP. *Manual of Photogrammetry.* American Society for Photogrammetry, 4th edition, 1984.
2. B. Caprile and V. Torre. Using vanishing points for camera calibration. *International Journal of Computer Vision*, 4:127–140, April 1990.
3. T. Echigo. A camera calibration technique using three sets of parallel lines. *Machine Vision and Applications*, 3:159–167, March 1990.
4. K. Kanatani and Y. Onodera. Noise robust camera calibration using vanishing points. *IEICE Transaction on Information and Systems*, E74(10), October 1991.
5. J. M. Lavest, G. Rives, and M. Dhome. 3D reconstruction by zooming. *IEEE Robotics and Automation (to appear)*, 1993.
6. M. X. Li. Camera calibration of the KTH head-eye system. Technical report, CVAP-147, NADA, KTH., March 1994.
7. M.X. Li and Demetrios Betsis. Kinematic calibration of a binocular head-eye system for active vision. Technical report, (in prep.), CVAP, NADA, KTH, 1994.
8. K. Pahlavan and J.O. Eklundh. A head-eye system – analysis and design. *CVGIP: Image Understanding*, 56(1):41–56, July 1992.
9. K. Pahlavan, T. Uhlin, and J.O. Eklundh. Active vision as a methodology. In J. Y. Aloimonos, editor, *Active Perception*, Advances in Computers. Lawrence-Erlbaum, 1993.
10. K. Tarabanis, R. Y. Tsai, and D. S. Goodman. Modeling of a computer-controlled zoom lens. In *IEEE Iinternational Conference on Robotics and Automation*, pages 1545–1551, Nice, France, May 1992.
11. Roger Y. Tsai. A versatile camera calibration technique for high-accuracy 3D machine vision metrology using off-the-shelf TV cameras and lenses. *IEEE Joural of Robotics and Automation*, RA-3(4):323–331, August 1987.
12. L. Wang and W. Tsai. Computing camera parameters using vanishing-line information from a rectangular parallelepiped. *Machine Vision and Applications*, 3:129–141, March 1990.